Gas motion induced by unsteady boundary heating in a small-scale slab

Avshalom Manela[1] and Nicolas G. Hadjiconstantinou[2]
[1]*Department of Mathematics, Massachusetts Institute of Technology, Cambridge, Massachusetts 02139, USA*
[2]*Department of Mechanical Engineering, Massachusetts Institute of Technology, Cambridge, Massachusetts 02139, USA*

(Received 14 July 2008; accepted 9 October 2008; published online 17 November 2008)

We study the response of a gas confined in a small-scale gap to a small time-dependent change in the temperature of the gap boundaries. Using the collisionless Boltzmann equation, a general scheme for the calculation of the probability density function and the respective hydrodynamic fields in response to any heating history is developed. Asymptotic analytical results are obtained for the cases of "ramp" (linearly varying with a cutoff value) and oscillatory boundary heating. The ramp solution can be used to approximate the system response to arbitrarily slow and fast process time scales (compared to the mean free time) and thus complement previous analyses focusing on relatively slow or instantaneous heating. For oscillatory heating at frequencies significantly higher than the collision frequency, we find that, at late times, the hydrodynamic fields decay proportionally to $\exp[-(\omega\delta_w)^{2/3}]$, where ω is the oscillation frequency and δ_w is the distance from the wall. As a result, for sufficiently high frequencies, the steady-state gas motion is confined to narrow "bounded" layers in the vicinity of each wall. The results are compared with low-variance particle simulations of the linearized Boltzmann equation using the recently developed low-variance deviational simulation Monte Carlo method. Good agreement is found between the analysis and simulations, suggesting the former to be an accurate and simple means for calculating the hydrodynamic response of systems of arbitrary size within one mean free path from the heated boundary. © *2008 American Institute of Physics*. [DOI: 10.1063/1.3010759]

I. INTRODUCTION

The analysis of the time response of a fluid confined in a slab and subject to a change in the thermal properties of its boundaries is of both fundamental and practical importance in classical fluid mechanics[1] as well as in rarefied gas dynamics.[2] The fluid motion induced in this problem is driven by the mechanism of thermal expansion, which couples the temperature variations induced in the fluid with the appearance of density gradients. The problem of gradual change in wall thermal properties was studied in the context of continuum gas dynamics in a series of works by Radhwan and Kassoy[3] and Clarke *et al.*[4] To justify their use of continuum gas description, a time scale longer than some modest multiple of the mean free time between molecular collisions was assumed. Considering shorter time scales for the variation in wall properties requires the consideration of molecular details of the gas, which are difficult to incorporate within a continuum description.

Several studies have investigated the problem in the limit of sudden temperature variations by examining the response of a dilute gas to instantaneous changes in wall temperature in the free-molecular and transition flow regimes.[5–9] In all of these studies, a discontinuous jump in the temperature of one or both confining walls is imposed and the flow field is followed through its new equilibrium state. The characteristic time scale for arriving at the new equilibrium is found to be of the order of the acoustic time scale (the ratio of the gap width to the most probable molecular speed of gas molecules). Analytical and numerical solutions to this problem based on a collisionless description[9] have been found to be in good agreement with direct Monte Carlo simulations of the Boltzmann equation[10] in systems where the effect of collisions is small.

In this work we aim to complement the above studies by considering the response of a confined dilute gas to an unsteady continuous change in the temperatures of its boundaries, characterized by an arbitrary (small or large) time scale. With this solution we wish to extend both existing continuum gas dynamics studies where a finite time scale is assumed, as well as molecular-gas-dynamics studies where only discontinuous temperature changes are analyzed. Clearly, the case of a continuous temperature change is of more physical relevance to various applications, including micro- and nano-electro-mechanical devices.[11–13] In addition, considering the impact of a gradually decreasing time scale may ultimately help in identifying the breakdown of the continuum description and clarify the transition to the free-molecular-flow regime.

In Sec. II the linearized microscopic problem for a collisionless gas is formulated in terms of a pair of coupled integral equations and a general scheme for obtaining numerical solutions of the resulting equations is described. The cases of "ramp" (linear temperature increase with a cutoff value) and oscillatory heating are studied in detail in Secs. III and IV, respectively. The analysis includes the development of analytical results for the early-time behavior of hydrodynamic fields. Analytical results describing the steady-state behavior in the case of high-frequency oscillatory heating are also obtained. In Sec. V our results are presented and compared with low-variance particle simulations of the linearized Boltzmann equation. These simulations are obtained using the recently developed[14,15] low-variance deviational simula-

tion Monte Carlo (LVDSMC) method, which achieves significantly reduced statistical uncertainty[16,17] compared to DSMC simulations[10] in low-signal problems such as the one studied here. The comparison between LVDSMC and our analytical results verifies that the present analysis may serve as an accurate and simple means for describing the hydrodynamic response of systems of arbitrary size within one mean free path from the heated boundary. We close with some concluding remarks (Sec. VI).

II. PROBLEM DESCRIPTION

A. Microscopic description

We consider a dilute-gas layer of molecular mass m and uniform density ρ_0 confined between two infinitely long diffusely reflecting walls placed in the (y^*,z^*) plane at $x^*=\pm L/2$ (* denotes a dimensional variable). The gas is initially at rest and in thermodynamic equilibrium with the confining walls at a temperature T_0. At time $t^*=0$ the right $(x^*=-L/2)$ and left $(x^*=L/2)$ walls are heated independently and uniformly with prescribed time dependencies, $T^*_{w_+}=T_0[1+\epsilon g_+(t^*)]$ and $T^*_{w_-}=T_0[1+\epsilon g_-(t^*)]$, respectively. It is assumed that $\epsilon \ll 1$ and $|g_\pm(t^*)| \sim O(1)$ so that the system description may be linearized about its initial equilibrium. To render the problem dimensionless we normalize position by L, velocity by the most probable molecular speed $U_{\mathrm{th}}=\sqrt{2RT_0}$, and density and temperature by ρ_0 and T_0, respectively. The resulting time scale is thus the acoustic scale $t_a=L/U_{\mathrm{th}}$. Here, $R=k_B/m$ is the specific gas constant, and k_B is the Boltzmann constant. For future reference, we define the Knudsen number[18]

$$\mathrm{Kn}=\frac{l}{L},$$

wherein $l=m/(\sqrt{2}\pi\rho_0 d^2)$ is the molecular mean free path and d is the "equivalent" hard-sphere diameter. The molecular collision time is given by $t_c=\sqrt{\pi}l/(2U_{\mathrm{th}})$.

The gas state is described by the probability density function

$$f(t,x,\mathbf{c})=F_M[1+\epsilon\phi(t,x,\mathbf{c})], \tag{1}$$

wherein $\mathbf{c}=(c_x,c_y,c_z)$ is the vector of molecular velocity, $F_M=\pi^{-3/2}\exp[-c^2]$ is the equilibrium Maxwellian distribution, and ϕ is the unknown perturbation. Neglecting the effects of molecular collisions, the linearized problem for ϕ is governed by the collisionless Boltzmann equation,[19]

$$\frac{\partial\phi}{\partial t}+c_x\frac{\partial\phi}{\partial x}=0, \tag{2}$$

together with the initial condition

$$\phi(t=0,x,\mathbf{c})=0 \tag{3}$$

and the linearized diffuse boundary conditions

$$\phi(t,x=\mp 1/2,c_x \gtrless 0)=\rho_\pm(t)+g_\pm(t)\left(c^2-\tfrac{3}{2}\right). \tag{4}$$

The functions $\rho_\pm(t)$ are yet to be determined [see Eqs. (8) and (9) *et seq.*]. Given the collisionless approximation, we expect the above model to provide a good description of the system response for times smaller than the collision time, $t^* \lesssim t_c$ ($t \lesssim \mathrm{Kn}$), or, equivalently, within a distance of one mean free path from the wall.

Taking the Laplace transform of Eq. (2) and using Eqs. (3) and (4) yield the solution

$$\hat{\phi}(s,x,c_x \gtrless 0,c_y,c_z)=\left[\hat{\rho}_\pm(s)+\hat{g}_\pm(s)\left(c^2-\frac{3}{2}\right)\right]\times\exp\left[-\frac{s}{c_x}\left(x\pm\frac{1}{2}\right)\right], \tag{5}$$

where s is the Laplace variable and $\hat{}$ denotes the Laplace transform of a function. By inversion of Eq. (5) we obtain

$$\phi(t,x,c_x \gtrless 0,c_y,c_z)=\rho_\pm(t_\pm)+g_\pm(t_\pm)\left(c^2-\tfrac{3}{2}\right), \tag{6}$$

where $t_\pm=t-(x\pm 1/2)/c_x$ are the retarded times corresponding to the signals generated at time t at the walls $x=\mp 1/2$, respectively.

The fields $\rho_\pm(t)$ are determined by imposing impermeability conditions at the walls,

$$\int_{-\infty}^{\infty} c_x\phi\left(x=\mp\frac{1}{2}\right)Fd\mathbf{c}=0. \tag{7}$$

Substituting Eq. (6) into Eq. (7) yields a pair of coupled integral equations,

$$\rho_-(t)-\int_0^t\frac{d\rho_+}{d\tau}\exp\left[-\frac{1}{(t-\tau)^2}\right]d\tau=2\int_0^t\frac{g_+(\tau)}{(t-\tau)^3}\left[\frac{1}{(t-\tau)^2}-\frac{1}{2}\right]\exp\left[-\frac{1}{(t-\tau)^2}\right]d\tau-\frac{1}{2}\left[g_-(t)+g_+(0)\exp\left(-\frac{1}{t^2}\right)\right], \tag{8}$$

$$\rho_+(t)-\int_0^t\frac{d\rho_-}{d\tau}\exp\left[-\frac{1}{(t-\tau)^2}\right]d\tau=2\int_0^t\frac{g_-(\tau)}{(t-\tau)^3}\left[\frac{1}{(t-\tau)^2}-\frac{1}{2}\right]\exp\left[-\frac{1}{(t-\tau)^2}\right]d\tau-\frac{1}{2}\left[g_+(t)+g_-(0)\exp\left(-\frac{1}{t^2}\right)\right] \tag{9}$$

which needs to be solved in conjunction with the initial conditions $\rho_+(0)=-g_+(0)/2$ and $\rho_-(0)=-g_-(0)/2$.

The key to obtaining a number of analytical results is to rewrite Eqs. (8) and (9) in terms of $\sigma(t)=\rho_+ +\rho_-$ and $\delta(t)=\rho_+-\rho_-$, which results in a pair of uncoupled equations,

$$\sigma(t)-\int_0^t\frac{d\sigma}{d\tau}\exp\left[-\frac{1}{(t-\tau)^2}\right]d\tau=2\int_0^t\frac{g_\sigma(\tau)}{(t-\tau)^3}\left[\frac{1}{(t-\tau)^2}-\frac{1}{2}\right]\exp\left[-\frac{1}{(t-\tau)^2}\right]d\tau-\frac{1}{2}\left[g_\sigma(t)+g_\sigma(0)\exp\left(-\frac{1}{t^2}\right)\right] \tag{10}$$

and

$$\delta(t) + \int_0^t \frac{d\delta}{d\tau}\exp\left[-\frac{1}{(t-\tau)^2}\right]d\tau = -2\int_0^t \frac{g_\delta(\tau)}{(t-\tau)^3}\left[\frac{1}{(t-\tau)^2}-\frac{1}{2}\right]\exp\left[-\frac{1}{(t-\tau)^2}\right]d\tau - \frac{1}{2}\left[g_\delta(t) - g_\delta(0)\exp\left(-\frac{1}{t^2}\right)\right], \tag{11}$$

where $g_\sigma(t)=g_+ + g_-$ and $g_\delta(t)=g_+ - g_-$. These are supplemented by the initial conditions $\sigma(0)=-g_\sigma(0)/2$ and $\delta(0)=-g_\delta(0)/2$.

For the simplified case of $g_+=1$ and $g_-=R_\epsilon$ (constant), corresponding to $g_\sigma=1+R_\epsilon$ and $g_\delta=1-R_\epsilon$, the authors have developed in previous work[9] an analytical solution for the distribution function representing the case of step boundary-temperature change.

B. Numerical scheme for solution of Eqs. (8) and (9)

The above pair of equations is also a convenient starting point for a simple numerical method for treating arbitrary $g_\pm(t)$. To solve for $\sigma(t)$ and $\delta(t)$ we make use of the following simple Euler-type method by casting Eqs. (10) and (11) in the form

$$F(t) - k_1\int_0^t \frac{dF}{d\tau}\exp\left[-\frac{1}{(t-\tau)^2}\right]d\tau = G(t), \tag{12}$$

with $F(t)$ either $\sigma(t)$ or $\delta(t)$, together with $F(0)=k_2$ [constants k_1 and k_2 determined from Eq. (10) or (11)].

Our goal is to determine $F(t)$ by discretizing time using a series of time steps $t_{n+1}=t_n+\Delta t$ coupled with the approximation

$$F(t_{n+1}) \approx F(t_n) + \left(\frac{dF}{dt}\right)_{t_n}\Delta t + O(\Delta t^2).$$

To obtain an expression for $(dF/dt)_{t_n}$ we approximate the integral term in Eq. (12) by

$$I_n = \int_0^{t_n}\frac{dF}{d\tau}\exp\left[-\frac{1}{(t_n-\tau)^2}\right]d\tau \approx \left(\frac{dF}{dt}\right)_{t_0=0}\int_0^{t_1}\exp\left[-\frac{1}{(t_n-\tau)^2}\right]d\tau + \cdots + \left(\frac{dF}{dt}\right)_{t_{n-1}}\int_{t_{n-1}}^{t_n}\exp\left[-\frac{1}{(t_n-\tau)^2}\right]d\tau, \tag{13}$$

which, after collecting terms, yields

$$\left(\frac{dF}{dt}\right)_{t_n} \approx \frac{G(t_{n+1}) - F(t_n) + k_1\sum_{i=0}^{n-1}\left(\frac{dF}{dt}\right)_{t_i}\int_{t_i}^{t_{i+1}}\exp\left[-\frac{1}{(t_{n+1}-\tau)^2}\right]d\tau}{\Delta t - k_1\int_{t_n}^{t_{n+1}}\exp\left[-\frac{1}{(t_{n+1}-\tau)^2}\right]d\tau}. \tag{14}$$

While there are numerical procedures far more sophisticated for integrating Eqs. (10) and (11), we deliberately apply here a very simple scheme to demonstrate its effectiveness in providing accurate solutions of the problem (see Sec. V).

C. Expressions for the hydrodynamic fields

Once ϕ is known, the $O(\epsilon)$ perturbations of the hydrodynamic fields may be calculated by appropriate quadratures over the molecular velocity space.[19] Introducing

$$\Phi_\pm^n = \int_{c_{x_\pm}}^{\pm\infty} g_\pm(t_\pm)c_x^n\exp[-c_x^2]dc_x, \qquad \Psi_\pm^n = \int_{c_{x_\pm}}^{\pm\infty}\rho_\pm(t_\pm)c_x^n\exp[-c_x^2]dc_x, \tag{15}$$

with $c_{x_\pm}=(x\pm 1/2)/t$, the $O(\epsilon)$ density, x-component velocity, temperature, and x-component heat-flux perturbations are, respectively, expressed as

$$\rho = \frac{1}{\sqrt{\pi}}\left[\Psi_+^0 - \Psi_-^0 + \Phi_+^2 - \Phi_-^2 - \frac{1}{2}(\Phi_+^0 - \Phi_-^0)\right], \tag{16}$$

$$u_x = \frac{1}{\sqrt{\pi}}\left[\Psi_+^1 - \Psi_-^1 + \Phi_+^3 - \Phi_-^3 - \frac{1}{2}(\Phi_+^1 - \Phi_-^1)\right], \tag{17}$$

$$T = \frac{2}{3\sqrt{\pi}}\left[\Psi_+^2 - \Psi_-^2 - \frac{1}{2}(\Psi_+^0 - \Psi_-^0) + \Phi_+^4 - \Phi_-^4 - \Phi_+^2 + \Phi_-^2 + \frac{5}{4}(\Phi_+^0 - \Phi_-^0)\right], \tag{18}$$

and

$$q_x = \frac{1}{2\sqrt{\pi}}\left[\Psi_+^3 - \Psi_-^3 + \Psi_+^1 - \Psi_-^1 + \Phi_+^5 - \Phi_-^5 + \frac{1}{2}(\Phi_+^3 - \Phi_-^3) + \frac{1}{2}(\Phi_+^1 - \Phi_-^1)\right] - \frac{5}{4}u_x. \tag{19}$$

III. RAMP HEATING

Consider the case where the temperature of each wall varies linearly with a cutoff value, i.e.,

$$g_+(t) = \begin{cases} kt, & 0 \le t \le 1/k \\ 1, & t > 1/k \end{cases}$$
$$g_-(t) = \begin{cases} kR_\epsilon t, & 0 \le t \le 1/k \\ R_\epsilon, & t > 1/k, \end{cases} \tag{20}$$

where $R_\epsilon \sim O(1)$ and k are constants. This heating profile has been chosen because it can be used to bridge slow and fast heating processes as well as approximate either process in the appropriate limit. Although the collision time is very short in macroscopic units, similar fast processes have recently appeared in connection to a number of industrial applications.[12,13]

To obtain the system behavior at early times $0 \le t \le 1/k \ll 1$, we apply the scheme outlined in Sec. II B for one time step. The leading order behavior of ρ_+ and ρ_- is then found to be

$$\rho_+(t) \approx -\frac{1}{2}kt + O(\exp[-t^{-2}]),$$
$$\rho_-(t) \approx -\frac{R_\epsilon}{2}kt + O(\exp[-t^{-2}]). \tag{21}$$

Substituting Eqs. (20) and (21) into Eqs. (15)–(19) yields the early-time approximations for $0 \le t \le 1/k$,

$$\rho \approx \frac{k}{2\sqrt{\pi}}\left\{\left(x+\frac{1}{2}\right)\Gamma(0,c_{x_+}^2) - R_\epsilon\left(x-\frac{1}{2}\right)\Gamma(0,c_{x_-}^2) - \frac{\sqrt{\pi}}{2}t[\gamma(c_{x_+}) + R_\epsilon\gamma(-c_{x_-})]\right\}, \tag{22}$$

$$u_x \approx \frac{k}{4}\left[\left(x+\frac{1}{2}\right)\gamma(c_{x_+}) + R_\epsilon\left(x-\frac{1}{2}\right)\gamma(-c_{x_-})\right], \tag{23}$$

$$T \approx \frac{k}{6\sqrt{\pi}}\left\{\left(x+\frac{1}{2}\right)\exp[-c_{x_+}^2] - R_\epsilon\left(x-\frac{1}{2}\right)\exp[-c_{x_-}^2] + \frac{3\sqrt{\pi}}{2}t[\gamma(c_{x_+}) + R_\epsilon\gamma(-c_{x_-})]\right\} - \rho, \tag{24}$$

$$q_x \approx \frac{k}{2\sqrt{\pi}}\left\{\frac{1}{4}\left[\left(x+\frac{1}{2}\right)c_{x_+}\exp[-c_{x_+}^2] - R_\epsilon\left(x-\frac{1}{2}\right)c_{x_-}\exp[-c_{x_-}^2]\right] - \sqrt{\pi}\left[\left(x+\frac{1}{2}\right)\gamma(c_{x_+}) + R_\epsilon\left(x-\frac{1}{2}\right)\gamma(-c_{x_-})\right] + t\left\{\exp[-c_{x_+}^2] - R_\epsilon\exp[-c_{x_-}^2]\right\}\right\}, \tag{25}$$

where $\gamma(z) = (2/\sqrt{\pi})\int_z^\infty \exp[-p^2]dp$ is the complementary error function and $\Gamma(a,z) = \int_z^\infty p^{a-1}\exp[-p]dp$ is the upper incomplete gamma function.

For sufficiently rapid heating where $1/k \ll 1$, the early stage of constant boundary temperature, $1/k < t \ll 1$, may also be included in the early-time approximation. For $1/k < t \ll 1$ the leading order expressions for ρ_+ and ρ_- are

$$\rho_+(t) \approx -\frac{1}{2} + O(\exp[-t^{-2}]),$$
$$\rho_-(t) \approx -\frac{R_\epsilon}{2} + O(\exp[-t^{-2}]). \tag{26}$$

Since the expressions in Eq. (15) for $g_\pm$ and $\rho_\pm$ depend on c_x through the retarded times $t_\pm$, each of the quadratures in Eq. (15) naturally separates into two integrals. Substituting Eq. (20) into $\Phi_\pm^n$ in Eq. (15), we obtain

$$\Phi_+^n = k\int_{c_{x_+}}^{(x+1/2)/(t-1/k)} t_+ c_x^n \exp[-c_x^2]dc_x + \int_{(x+1/2)/(t-1/k)}^{\infty} c_x^n \exp[-c_x^2]dc_x \tag{27}$$

and

$$\Phi_-^n = R_\epsilon k\int_{c_{x_-}}^{(x-1/2)/(t-1/k)} t_- c_x^n \exp[-c_x^2]dc_x + R_\epsilon\int_{(x-1/2)/(t-1/k)}^{-\infty} c_x^n \exp[-c_x^2]dc_x. \tag{28}$$

Explicit formulas for Eqs. (27) and (28) are calculated in Appendix A. Substituting Eq. (21) and Eq. (26) into $\Psi_\pm^n$ in Eq. (15), we find that $\Psi_\pm^n \approx -\Phi_\pm^n/2$. Once $\Phi_\pm^n$ and $\Psi_\pm^n$ are known, Eqs. (16)–(19) yield the required early-time approximations for the macroscopic fields.

The above analysis may serve to complement results existing in literature for the system response to relatively slow boundary heating[3,4] and instantaneous temperature jump.[9] For completeness and for correcting typographical errors appearing in a previous work,[9] the early-time approximations corresponding to the latter case are included in Appendix B.

At late times $t \gg 1$ (and also $t \gg 1/k$), application of the final-value theorem yields the system final equilibrium state consisting of vanishing density and velocity perturbations, together with $T \approx (1+R_\epsilon)/2$ and $q_x \approx (1-R_\epsilon)/(2\sqrt{\pi})$.

IV. OSCILLATORY HEATING

For simplicity, we consider the case where the temperature of both walls oscillates with common amplitude and phase,

$$g_+(t) = g_-(t) = \sin(\omega t). \tag{29}$$

First we study the early-time response of the system at moderate frequencies, $\omega \lesssim 1$, and then calculate the steady-state solution[20] for $\omega \gg 1$.

A. The case $\omega \lesssim O(1)$

Applying the scheme in Sec. II B as described in the beginning of Sec. III, we find for the leading order behavior at $t \ll 1$

$$\rho_+(t) = \rho_-(t) \approx -\tfrac{1}{2}\sin(\omega t) + O(\exp[-t^{-2}]). \tag{30}$$

For $\omega \lesssim O(1)$ this is equivalent to a special case of the ramp heating problem discussed in Sec. III with $k=\omega$ and $R_\epsilon = 1$. The early-time approximations are therefore given by the corresponding expressions (22)–(25).

B. The case $\omega \gg 1$

Motivated by some of our numerical results (see Sec. V), we seek an analytical description of the steady-state behavior of the system at high frequencies. For $g_+(t)=g_-(t)=\sin(\omega t)$, Eq. (11) yields $\delta(t)\equiv 0$. Substituting Eq. (29) into Eq. (10), we find that $\sigma(t)$ satisfies

$$\begin{aligned}\sigma(t) - \int_0^t \frac{d\sigma}{d\tau}\exp\left[-\frac{1}{(t-\tau)^2}\right]d\tau \\ = 4\ \mathrm{Im}\left\{\int_0^t \frac{\exp(i\omega\tau)}{(t-\tau)^3}\left[\frac{1}{(t-\tau)^2}-\frac{1}{2}\right] \right. \\ \left. \times\exp\left[-\frac{1}{(t-\tau)^2}\right]d\tau\right\} - \sin(\omega t),\end{aligned} \tag{31}$$

where Im denotes the imaginary part of a complex number. Integration by parts shows that the integral term appearing on the right hand side of Eq. (31) is $O(\omega^{-1})$. Assuming a solution of the form $\sigma(t)\approx A\sin(\omega t)$, we find a similar estimation for the integral term appearing on the left hand side of Eq. (31). Consequently, for $\omega \gg 1$ we obtain $\sigma(t)\approx -\sin(\omega t)$ and thus

$$\rho_+(t) = \rho_-(t) \approx -\tfrac{1}{2}\sin(\omega t) + O(\omega^{-1}). \tag{32}$$

Substituting Eqs. (29) and (32) into Eq. (15), the integrals to be evaluated for the calculation of the macroscopic fields are

$$\Phi_\pm^n = \mathrm{Im}\left\{\exp[i\omega t]\int_{c_{x_\pm}}^{\pm\infty} c_x^n \exp\left[-c_x^2 - i\omega\frac{x\pm 1/2}{c_x}\right]dc_x\right\},$$
$$\Psi_\pm^n \approx -\frac{1}{2}\Phi_\pm^n, \tag{33}$$

where for steady state the lower limits of integration vanish ($|c_{x_\pm}| = |x\pm 1/2|/t \ll 1$). These steady-state quadratures may be approximated in cases where $\omega(1/2\pm x)\gg 1$. Applying the method of steepest descent[21] yields

$$\begin{aligned}\Phi_+^n &\approx \mathrm{Im}\left\{\sqrt{\frac{\pi}{3}}3^{-n/2}z_+^{n/2}\exp[i\omega t - z_+]\right. \\ &\left.\times[1 + a_1 z_+^{-1} + a_2 z_+^{-2} + O(z_+^{-3})]\right\}, \\ \Phi_-^n &\approx \mathrm{Im}\left\{\sqrt{\frac{\pi}{3}}(-1)^{n+1}3^{-n/2}z_-^{n/2}\exp[i\omega t - z_-]\right. \\ &\left.\times[1 + a_1 z_-^{-1} + a_2 z_-^{-2} + O(z_-^{-3})]\right\},\end{aligned} \tag{34}$$

where $z_\pm = 3[\omega(1/2\pm x)/2]^{2/3}\exp[i\pi/3]$, $a_1=(3n^2+3n-1)/12$, and $a_2=(9n^4+6n^3-51n^2-24n+25)/288$. The two correction terms in Eq. (34) become important in the vicinity of the walls where the product $\omega(1/2\pm x)$ may not satisfy $\omega(1/2\pm x)\gg 1$, because for any given $\omega\gg 1$, there always exists a region sufficiently close to the walls where $\omega(1/2\pm x)<1$ and Eq. (34) are not valid (see Fig. 6). Within these regions, of particular interest are the values of $\Phi_\pm^n$ at the walls, which can be easily calculated from Eq. (33) using the properties of $J_n(z)=\int_z^\infty p^n\exp[-p^2]dp$ given in Appendix A.

Substituting Eq. (33) into Eqs. (16)–(19), the high-frequency approximations for the macroscopic fields are

$$\rho \approx \frac{1}{\sqrt{\pi}}[(\Phi_+^2 - \Phi_-^2) - (\Phi_+^0 - \Phi_-^0)], \tag{35}$$

$$u_x \approx \frac{1}{\sqrt{\pi}}[(\Phi_+^3 - \Phi_-^3) - (\Phi_+^1 - \Phi_-^1)], \tag{36}$$

$$T \approx \frac{2}{3\sqrt{\pi}}\left[(\Phi_+^4 - \Phi_-^4) - \frac{3}{2}(\Phi_+^2 - \Phi_-^2) + \frac{3}{2}(\Phi_+^0 - \Phi_-^0)\right], \tag{37}$$

$$q_x \approx \frac{1}{2\sqrt{\pi}}(\Phi_+^5 - \Phi_-^5) - \frac{5}{4}u_x. \tag{38}$$

The following simple expressions follow at the walls:

$$\begin{aligned}\rho\left(x=\pm\frac{1}{2}\right) &\approx -\frac{1}{4}\sin(\omega t), \\ T\left(x=\pm\frac{1}{2}\right) &\approx \frac{1}{2}\sin(\omega t), \\ q_x\left(x=\pm\frac{1}{2}\right) &\approx \mp\frac{1}{2\sqrt{\pi}}\sin(\omega t),\end{aligned} \tag{39}$$

together with a vanishing velocity.

V. RESULTS AND DISCUSSION

We validate our results by comparing them with *low-variance* Monte Carlo solutions of the linearized Boltzmann equation for a hard-sphere gas obtained using the recently developed[14,15] LVDSMC method. LVDSMC is a particle method akin to DSMC, which uses variance reduction

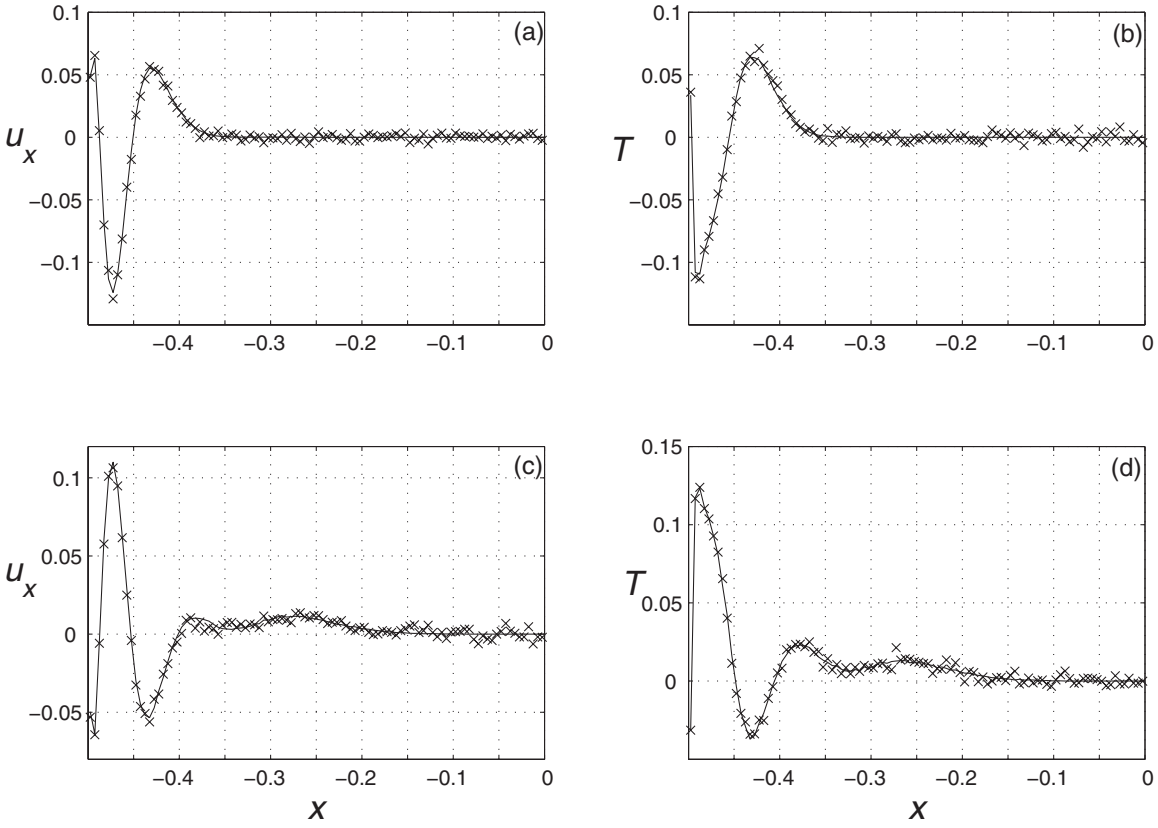

FIG. 1. Comparison between DSMC (crosses) and LVDSMC (solid line) solutions for the [(a) and (c)] velocity and [(b) and (d)] temperature perturbations for oscillatory heating with $\omega=40\pi$ and Kn=1 at $-0.5\leq x\leq 0$ and times [(a) and (b)] $t=0.055$ and [(c) and (d)] $t=0.13$.

ideas[16] to significantly reduce the statistical uncertainty in sampled hydrodynamic quantities in cases where the deviation from equilibrium is small, as in the present problem. The reduced statistical uncertainty facilitates a closer comparison between theory and simulation. More importantly, in some cases it enables the study of low-signal flows that would have been impossible using DSMC. This is the case here, where the simulation of the $k\sim O(1)$ ramp heating and $\omega\sim O(1)$ oscillatory heating at a low statistical uncertainty is impossible using DSMC with our current computational resources.

As shown in Ref. 15, when using similar discretization, the LVDSMC method produces solutions in excellent agreement with their DSMC counterparts. This may have been anticipated since the LVDSMC method is rigorously derived from the Boltzmann equation and uses the same basic numerical ingredients as DSMC. In fact, LVDSMC differs from DSMC only in ways necessary for simulating the deviation from equilibrium. To verify this assertion and justify our subsequent use of LVDSMC, we performed comparisons between LVDSMC and DSMC solutions using the same discretization. These comparisons were performed for problems where DSMC solutions were feasible (albeit expensive), e.g., oscillatory heating with $\omega\gg 1$. Very good agreement was found in all cases examined. One representative example is shown in Fig. 1 in which the velocity and temperature fields are compared for the oscillatory case with $\omega=40\pi$ and Kn=1. Due to the smaller signal-to-noise ratio in the DSMC results, the latter calculation was performed with $\epsilon=0.04$, whereas the LVDSMC calculation was performed with $\epsilon=0.02$. Despite the visible statistical uncertainty in the DSMC solution, the agreement between the two solutions is very good.

In accordance with our problem description, diffuse boundary conditions are used for the simulations. The gas is initially at equilibrium with the wall temperature T_0. At $t^*\geq 0$ each wall temperature varies according to the prescribed $g_{\pm}(t)$ and the time evolution of the system is calculated. The simulation time step was chosen to be $1/(10n_{\text{cell}})$, where n_{cell} is the number of spatial cells. For the majority of calculations $n_{\text{cell}}=100$, except for the $\omega\gg 1$ case where $n_{\text{cell}}=200$ was used due to the rapid spatial variation in the solution. All LVDSMC calculations were performed with $\epsilon=0.02$. Our previous work[9] suggests that nonlinear effects become important at $\epsilon\approx 0.1$.

A. Ramp heating

Figure 2 describes the evolution of the hydrodynamic perturbation fields (16)–(19) for the ramp case with $k=R_\epsilon=1$ at the indicated values of t. The crosses correspond to LVDSMC results at $\text{Kn}\to\infty$, and the thin lines mark the late-time collisionless limit (see Sec. III). For this choice of R_ϵ, $\rho_+\equiv\rho_-$ [see Eqs. (8) and (9)] and thus density and temperature perturbations are symmetric while the velocity and heat flux are antisymmetric about $x=0$.

At early times ($t\ll 1$) both density and velocity disturbances propagate in a wavelike manner from the walls with

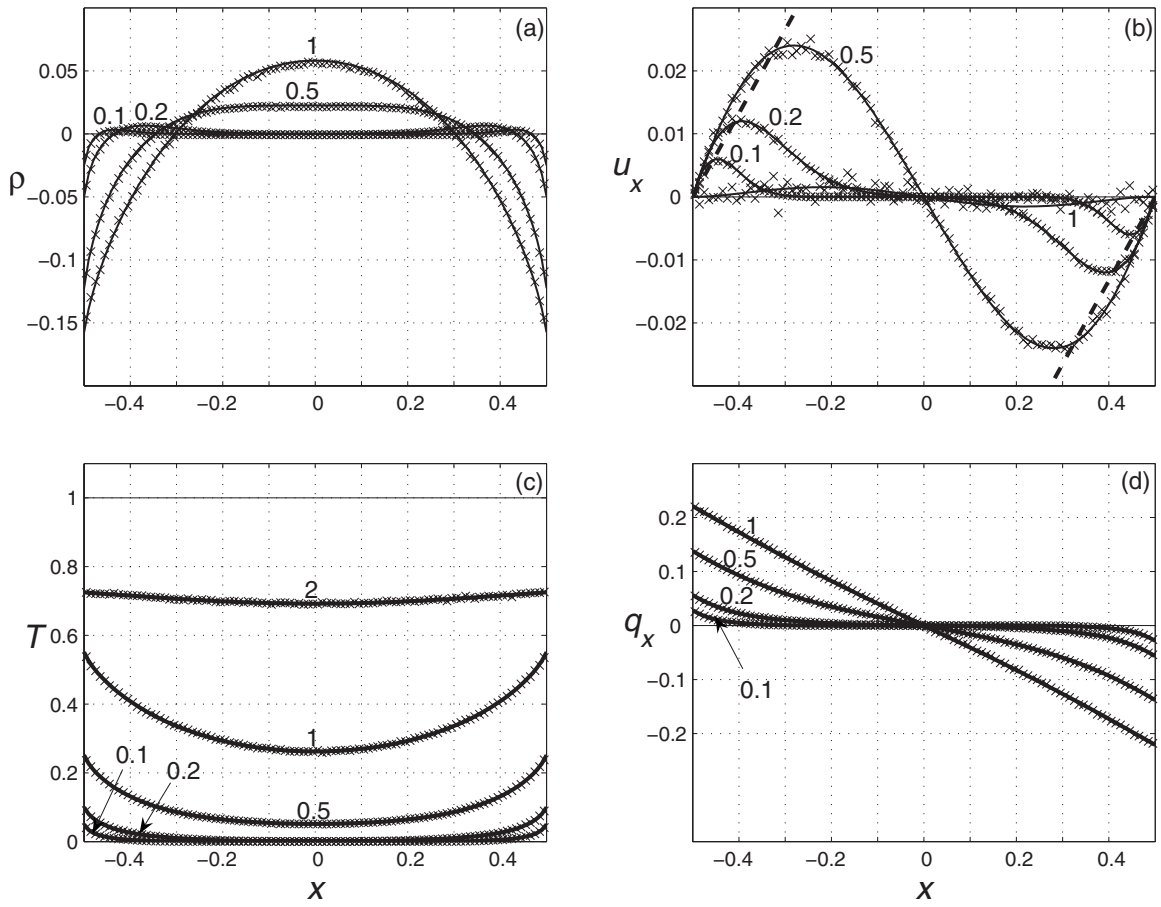

FIG. 2. The (a) density, (b) velocity, (c) temperature, and (d) heat-flux perturbation distributions for $k=R_\epsilon=1$ and the indicated values of time (solid lines). The crosses correspond to LVDSMC results at $\mathrm{Kn}\to\infty$ and the thin solid lines mark the long-time collisionless limit (Sec. III). The dashed lines in (b) denote the early-time approximation (40) for the loci and amplitudes of the wave extrema.

approximately constant speed and increasing amplitude. At these times, expressions (22)–(25) provide results that are indistinguishable from the numerical solution outlined in Sec. II. The left- and right-traveling velocity-disturbance extrema are predicted by Eq. (23) to be

$$u_{x_{\mathrm{left}}}\left(x=-\frac{1}{2}+\frac{\sqrt{\pi}t}{4}\right)\approx\frac{\sqrt{\pi}kt}{16}\gamma\left(\frac{\sqrt{\pi}}{4}\right),$$
$$u_{x_{\mathrm{right}}}\left(x=\frac{1}{2}-\frac{\sqrt{\pi}t}{4}\right)\approx-\frac{\sqrt{\pi}kt}{16}\gamma\left(\frac{\sqrt{\pi}}{4}\right), \tag{40}$$

respectively, and are denoted by the dashed lines in Fig. 2(b). These are qualitatively different from the faster (extrema locations $\approx\mp 0.5\pm t$) constant-amplitude [$\approx 1/(2\sqrt{\pi e})$] waves predicted[9] in the instantaneous heating response [see Eq. (B2) with $R_\epsilon=1$].

At $t\approx 0.3$ the two waves adjoin for the first time while their magnitudes keep increasing. At $t=1$ the temperatures at both walls reach their cutoff value, and at later times the gas approaches its new equilibrium state through a series of decaying waves propagating across the slab. At the latest time presented ($t=2$), the density, velocity, and heat-flux perturbations are relatively small (not shown for clarity) while the temperature is still evolving toward its final value.

In view of the vastly different methods of calculation, the close agreement between the present analysis and LVDSMC results is gratifying. In contrast with the relatively costly numerical procedure and the inevitable appearance of statistical noise (visible even in the present low-noise LVDSMC calculations, e.g., the scatter of results in the velocity field), the present solution has the evident advantage of requiring very small computational effort.

To study the validity of the numerical scheme and early-time approximation to lower Knudsen number flows, Fig. 3 presents a comparison of the time evolution of the velocity and temperature perturbations at a fixed location, $x=-0.45$, with LVDSMC calculations at various Knudsen numbers for $k=R_\epsilon=1$. The solid lines denote the numerical solution (Sec. III), the dashed curves mark the early-time approximations (23) and (24), and the crosses, circles, and triangles, respectively, correspond to LVDSMC results at $\mathrm{Kn}=10$, 1, and 0.1. The early-time approximation coincides with the numerical results until $t\approx 0.4$ for the velocity and $t\approx 0.7$ for the temperature. The agreement with the $\mathrm{Kn}=10$ results is very good at all times presented. With decreasing Kn (and thus longer t^* corresponding to the same value of the nondimensional time t) we expect the agreement to become confined to lower values of t owing to the increasing effect of collisions. We thus regard the close agreement in the $\mathrm{Kn}=0.1$ case for

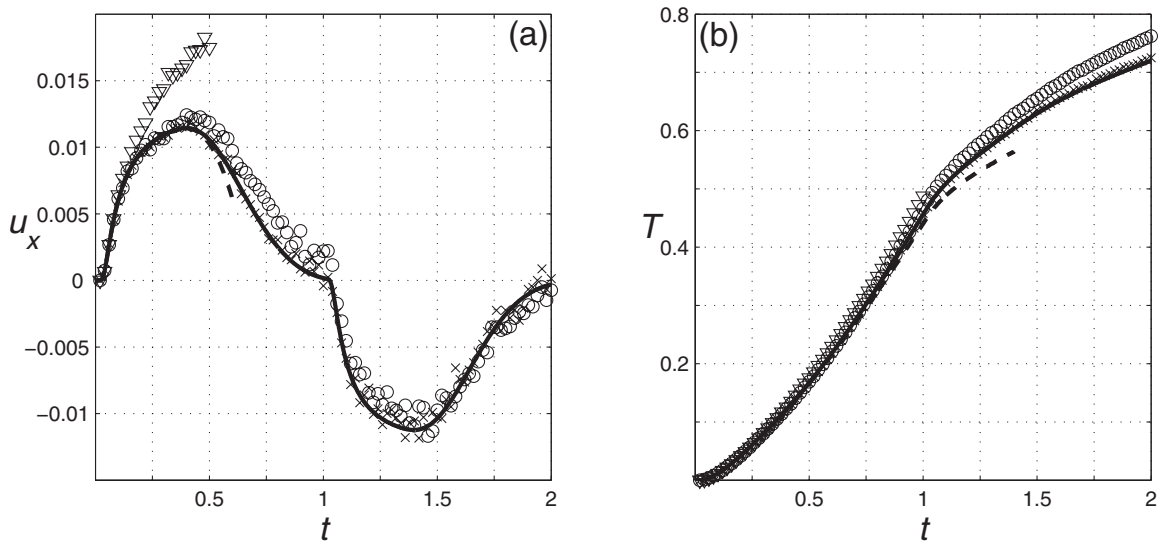

FIG. 3. Time evolution of the (a) velocity and (b) temperature perturbations at $x=-0.45$ for $k=R_\epsilon=1$. The crosses, circles, and triangles, respectively, correspond to LVDSMC results at Kn=10, 1, and 0.1. The dashed lines mark the early-time approximations obtained from Eqs. (23) and (24) ($t\leq 1$) and Appendix A ($t>1$).

the temperature up to $t=1$ as remarkable, and perhaps, fortuitous. Nevertheless, the existence of an initial time interval $t\lesssim \mathrm{Kn}$ where the collisionless analysis is valid is clearly demonstrated.

To further validate the early-time approximation, Fig. 4 presents a similar comparison for $k=20$ and $R_\epsilon=1$, where the wavelike time variation in the velocity field is visible. The flow velocity magnitude, however, is rapidly damped and equilibrium is achieved after a few acoustic times. For this $k\gg 1$ case, the $t\ll 1$ approximation consists of Eqs. (22)–(25) for $t\leq 0.05$ and the expressions in Appendix A for $t>0.05$ (see also Sec. III). The agreement with both numerical and LVDSMC results for Kn=10 and Kn=1 is very good for $t\lesssim 0.4$. As in Fig. 3, even for Kn=0.1 there exists an initial time interval $t\lesssim \mathrm{Kn}$ where the collisionless calculation is valid. This suggests the present analysis as a viable means for providing a quantitative description of the initial transient in the counterpart continuum-limit problem.

B. Oscillatory heating

We focus on the high-frequency ($\omega\gg 1$) case analyzed in Sec. IV B. The steady-state expressions (34) obtained for $\Phi^n_\pm$ indicate that the amplitude Δ of the hydrodynamic fields decays with the distance from the wall, δ_w, according to $\Delta\sim\exp[-(\omega\delta_w)^{2/3}]$. As a result, for sufficiently high oscillation frequencies, hydrodynamic activity is confined to thin bounded layers in the immediate vicinity of the walls. This behavior is similar to a previously studied phenomenon in high-frequency oscillatory shear driven flows.[22,23] The time

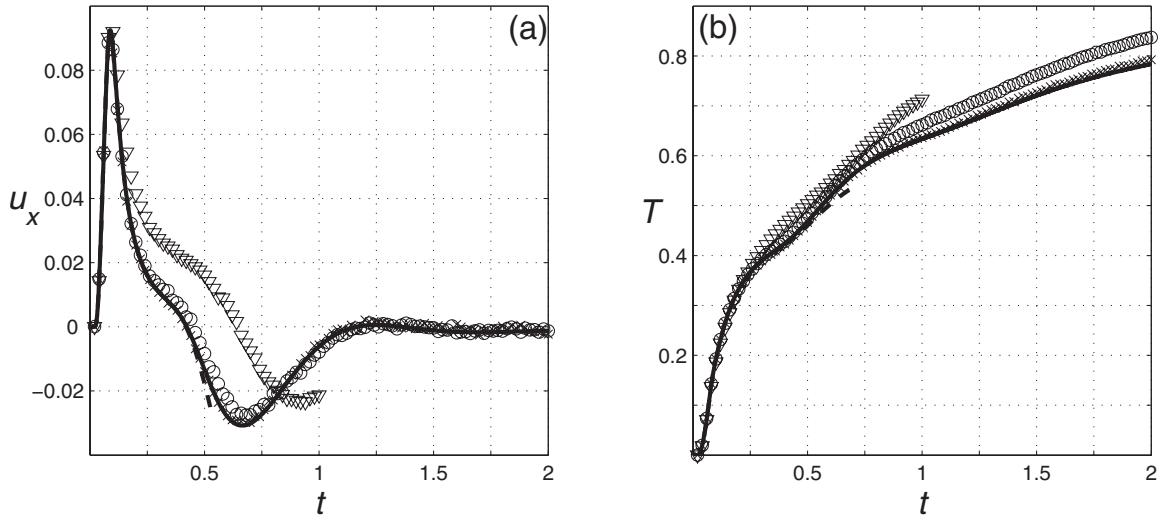

FIG. 4. Time evolution of the (a) velocity and (b) temperature perturbations at $x=-0.45$ for $k=20$ and $R_\epsilon=1$. The crosses, circles, and triangles, respectively, correspond to LVDSMC results at Kn=10, 1, and 0.1. The dashed lines mark the early-time approximations obtained from Eqs. (23) and (24) ($t\leq 0.05$) and Appendix A ($t>0.05$).

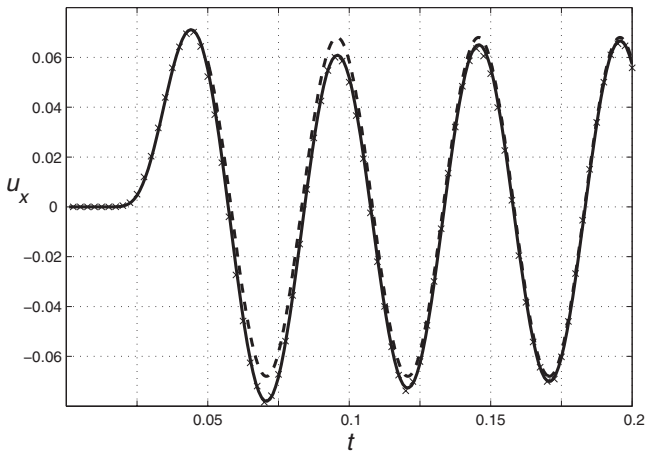

FIG. 5. Time evolution of the velocity distribution at $x=-0.45$ for $\omega=40\pi$. The solid and dashed lines, respectively, correspond to the numerical (Sec. II) and steady-state (Sec. IV B) solutions and the crosses mark the LVDSMC results at Kn=1.

t_s expected for the system to establish a steady state at a given distance δ_w from the boundary is $t_s \gg \delta_w$. Note again that approximation (34) is valid for $\omega\delta_w \gg 1$, while at the walls Eq. (39) should be applied.

To demonstrate the transition to steady state at a given location, Fig. 5 shows the velocity field at $x=-0.45$ ($\delta_w=0.05$) for the case $\omega=40\pi$. The solid and dashed lines, respectively, correspond to the numerical (Sec. II) and steady-state (Sec. IV B) solutions, and the crosses mark LVDSMC results at Kn=1. The agreement between LVDSMC and numerical calculations is very good at all times. At $t\approx 0.18$, slightly before four periods of the boundary conditions are completed, both results match with the dashed curve and a steady state is established. This is in accordance with the above estimate for the settling time, $t_s \gg \delta_w$.

Further comparison between the steady-state and LVDSMC solutions is made in Fig. 6. The solid lines correspond to the analytical approximations for the velocity and temperature perturbations, and the crosses denote LVDSMC results for Kn=1, $\omega=40\pi$, and $t=0.475$. The x-axis range is limited to the approximate width of the left-wall layer, $-0.5 \le x \le -0.25$. Symmetric results are obtained near the right wall. Good agreement is observed throughout the layer except for the very proximity of the wall where the product $\omega\delta_w$ is no longer large. The circles mark the values (39) of the hydrodynamic perturbations at the wall.

From Eq. (34) we see that the bounded layer width decreases with increasing ω. This suggests that for sufficiently large ω the system evolution will be entirely determined by a collisionless description regardless of its size. Motivated by the comparison of Fig. 6, Fig. 7 investigates the ability of the analytical steady-state solution to describe such systems; specifically, Fig. 7(a) compares analytical results with LVDSMC simulations at various Kn for $\omega=40\pi$, whereas Fig. 7(b) treats the case of $\omega=100\pi$. The results demonstrate that with increasing ω the collisionless analysis better captures the behavior of larger systems: while the agreement in the $\omega=40\pi$ case is less satisfactory already at Kn=0.1, the steady-state $\omega=100\pi$ results are in good agreement even for Kn=0.04. It is therefore concluded that with further increasing ω the effect of collisions becomes negligible and the present analysis provides a satisfactory description of the system behavior at all times.

VI. CONCLUDING REMARKS

In this work we have studied the response of a gas confined in a small-scale gap to a time-dependent arbitrary small change in the temperature of its boundaries, under the assumption of diffuse boundary conditions. This choice of boundary conditions was motivated by previous work (see Ref. 18), which suggests that for engineering surfaces diffuse boundary conditions are a reasonable approximation. In

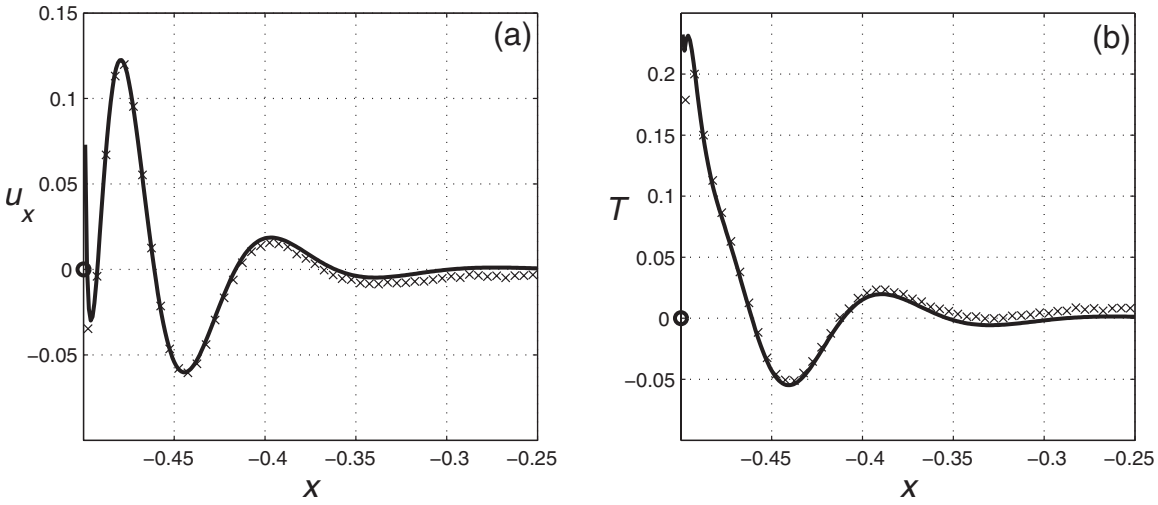

FIG. 6. The steady-state (a) velocity and (b) temperature perturbation distributions (solid lines) for $\omega=40\pi$ at $t=0.025+0.05n$ ($n \gg 1$). The crosses correspond to LVDSMC results at Kn=1 and $t=0.475$ and the circles mark the values in Eq. (39) at the wall.

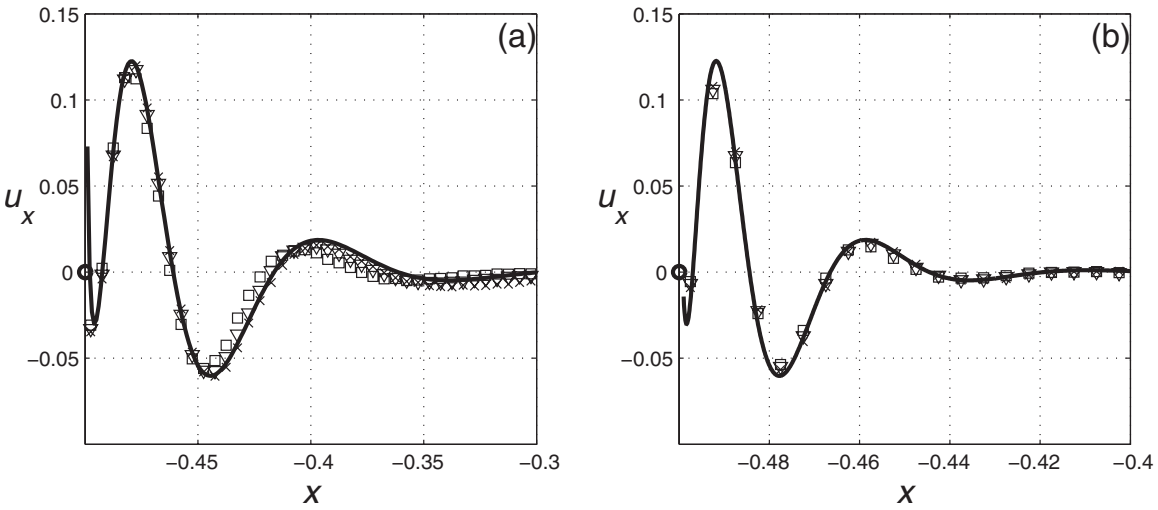

FIG. 7. The steady-state velocity distribution (solid lines) for (a) $\omega=40\pi$ ($t=0.475$) and (b) $\omega=100\pi$ ($t=0.49$), respectively. The crosses, triangles, and squares correspond to LVDSMC results for Kn=1, 0.1, and 0.04, respectively. The circles mark the theoretical values at the wall.

practice, microscopic gas-surface interactions are more complex and may be better described by incorporating several phenomenological accommodation coefficients.[19] Perhaps the simplest generalization of the present work would consist of replacing the diffuse boundary conditions with the Maxwell model, according to which a fraction $0\leq\alpha\leq1$ of the molecules are reflected diffusely while the remaining molecules undergo specular reflection. This would require replacing Eq. (4) in Sec. II with the condition

$$\phi(t,x=\mp1/2,c_x\gtrless0) = \alpha\left[\rho_{\pm}(t)+g_{\pm}(t)\left(c^2-\frac{3}{2}\right)\right] + (1-\alpha)\phi(t,x=\mp1/2,c_x\lesseqgtr0). \tag{41}$$

Without going further into the details of calculation, this modification is expected to reduce the boundary influence on the gas state.

By studying the gas response to arbitrary small changes in the temperature of its boundaries, we have complemented existing studies limited to slow heating or discontinuous temperature changes. Although the present analysis was carried out for a collisionless gas, the results obtained prove to be of practical relevance in several cases. First, they provide the early-time behavior of systems of arbitrary size and may therefore be useful for prescribing the initial system response in counterpart continuum-limit analyses. Second, in cases where the effect of the boundaries does not exceed more than one mean free path into the gas (e.g., the high-frequency oscillatory case discussed in Sec. IV B and Figs. 5–7), the effect of collisions is negligible, and the present analysis provides an accurate and simple description at all times.

APPENDIX A: EVALUATION OF EQS. (27) AND (28)

Substituting $t_{\pm}=t-(x\pm1/2)/c_x$ into Eqs. (27) and (28), we write

$$\Phi_+^n = kt\int_{c_{x_+}}^{\bar{c}_{x_+}} c_x^n\exp[-c_x^2]dc_x - k\left(x+\frac{1}{2}\right) \times\int_{c_{x_+}}^{\bar{c}_{x_+}} c_x^{n-1}\exp[-c_x^2]dc_x + \int_{\bar{c}_{x_+}}^{\infty} c_x^n\exp[-c_x^2]dc_x \tag{A1}$$

and

$$\Phi_-^n = R_\epsilon kt\int_{c_{x_-}}^{\bar{c}_{x_-}} c_x^n\exp[-c_x^2]dc_x - R_\epsilon k\left(x-\frac{1}{2}\right) \times\int_{c_{x_-}}^{\bar{c}_{x_-}} c_x^{n-1}\exp[-c_x^2]dc_x + R_\epsilon\int_{\bar{c}_{x_-}}^{-\infty} c_x^n\exp[-c_x^2]dc_x, \tag{A2}$$

where $\bar{c}_{x_\pm}=(x\pm1/2)/(t-1/k)$. Denoting

$$J_n(z)=\int_z^\infty p^n\exp[-p^2]dp,$$

we find that

$$\Phi_+^n = kt[J_n(c_{x_+})-J_n(\bar{c}_{x_+})]-k\left(x+\frac{1}{2}\right)[J_{n-1}(c_{x_+}) - J_{n-1}(\bar{c}_{x_+})]+J_n(\bar{c}_{x_+}) \tag{A3}$$

and

$$\Phi_-^n = (-1)^{n+1} R_\epsilon \left\{ kt[J_n(-c_{x_-}) - J_n(-\bar{c}_{x_-})] + k\left(x - \frac{1}{2}\right) \times [J_{n-1}(-c_{x_-}) - J_{n-1}(-\bar{c}_{x_-})] + J_n(-\bar{c}_{x_-}) \right\}. \quad \text{(A4)}$$

The quadratures in Eqs. (A3) and (A4) for $n=0,1,\ldots,5$ are evaluated by noting that [see Eqs. (22)–(25) *et seq.*]

$$J_{-1}(z) = \frac{1}{2}\Gamma(0,z^2), \quad J_0(z) = \frac{\sqrt{\pi}}{2}\gamma(z), \quad J_1 = \frac{1}{2}\exp[-z^2]$$

and applying the recurrence relation

$$J_n(z) = \frac{z^{n-1}}{2}\exp[-z^2] + \frac{n-1}{2}J_{n-2}, \quad n \geq 2.$$

APPENDIX B: EARLY-TIME APPROXIMATIONS FOR THE INSTANTANEOUS JUMP PROBLEM

The early-time approximations for the hydrodynamic fields in the instantaneous temperature jump (unit jump at $x=-1/2$ and R_ϵ at $x=1/2$) problem are [cf. Eqs. (2.25)–(2.28) in Ref. 9]

$$\rho \approx \frac{1}{2\sqrt{\pi}}\left\{ c_{x_+}\exp[-c_{x_+}^2] - R_\epsilon c_{x_-}\exp[-c_{x_-}^2] - \frac{\sqrt{\pi}}{2}[\gamma(c_{x_+}) + R_\epsilon\gamma(-c_{x_-})] \right\}, \quad \text{(B1)}$$

$$u_x \approx \frac{1}{2\sqrt{\pi}}\{c_{x_+}^2\exp[-c_{x_+}^2] - R_\epsilon c_{x_-}^2\exp[-c_{x_-}^2]\}, \quad \text{(B2)}$$

$$T \approx \frac{1}{3\sqrt{\pi}}\left\{ c_{x_+}^3\exp[-c_{x_+}^2] - R_\epsilon c_{x_-}^3\exp[-c_{x_-}^2] + \frac{3\sqrt{\pi}}{2}[\gamma(c_{x_+}) + R_\epsilon\gamma(-c_{x_-})] \right\}, \quad \text{(B3)}$$

$$q_x \approx \frac{1}{2\sqrt{\pi}}\left[\exp[-c_{x_+}^2]\left(\frac{1}{2}c_{x_+}^4 + c_{x_+}^2 + 1\right) - R_\epsilon\exp[-c_{x_-}^2] \times \left(\frac{1}{2}c_{x_-}^4 + c_{x_-}^2 + 1\right)\right] - \frac{5}{4}u_x. \quad \text{(B4)}$$

[1] H. Schlichting, *Boundary Layer Theory* (McGraw-Hill, New York, 1960).
[2] G. N. Patterson, *Introduction to the Kinetic Theory of Gas Flows* (University of Toronto, Toronto, 1971).
[3] A. M. Radhwan and D. R. Kassoy, "The response of a confined gas to thermal disturbance: Rapid boundary heating," J. Eng. Math. **18**, 133 (1984).
[4] J. F. Clarke, D. R. Kassoy, and N. Riley, "Shock waves generated in a confined gas due to rapid heat addition at the boundary. II Strong shock waves," Proc. R. Soc. London, Ser. A **393**, 331 (1984).
[5] Y. Sone, "Effect of sudden change of wall temperature in rarefied gas," J. Phys. Soc. Jpn. **20**, 222 (1965).
[6] L. Lees, "Kinetic theory description of rarefied gas flow," J. Soc. Ind. Appl. Math. **13**, 278 (1965).
[7] M. Perlmutter, "Analysis of transient heat transfer through a collisionless gas enclosed between parallel plates," ASME Paper No. 67-HT-53, 1967.
[8] D. C. Wadsworth, D. A. Erwin, and E. P. Muntz, "Transient motion of a confined rarefied gas due to wall heating or cooling," J. Fluid Mech. **248**, 219 (1993).
[9] A. Manela and N. G. Hadjiconstantinou, "On the motion induced in a small-scale gap due to instantaneous boundary heating," J. Fluid Mech. **593**, 453 (2007).
[10] G. Bird, *Molecular Gas Dynamics and the Direct Simulations of Gas Flows* (Clarendon, Oxford, 1994).
[11] D. Y. Tzou, *Macro-to-Microscale Heat Transfer* (Taylor & Francis, Washington, DC, 1997).
[12] C. M. Ho and Y. C. Tai, "Micro-electro-mechanical systems and fluid flows," Annu. Rev. Fluid Mech. **30**, 579 (1998).
[13] A. Haji-Sheikh, W. J. Minkowycz, and E. M. Sparrow, "Certain anomalies in the analysis of hyperbolic heat conduction," J. Heat Transfer **124**, 307 (2002).
[14] T. M. M. Homolle and N. G. Hadjiconstantinou, "Low-variance deviational simulation Monte Carlo," Phys. Fluids **19**, 041701 (2007).
[15] T. M. M. Homolle and N. G. Hadjiconstantinou, "A low-variance deviational simulation Monte Carlo for the Boltzmann equation," J. Comput. Phys. **226**, 2341 (2007).
[16] L. L. Baker and N. G. Hadjiconstantinou, "Variance reduction for Monte Carlo solutions of the Boltzmann equation," Phys. Fluids **17**, 051703 (2005).
[17] N. G. Hadjiconstantinou, A. L. Garcia, M. Z. Bazant, and G. He, "Statistical error in particle simulations of hydrodynamic phenomena," J. Comput. Phys. **187**, 274 (2003).
[18] N. G. Hadjiconstantinou, "The limits of Navier–Stokes theory and kinetic extensions for describing small-scale gaseous hydrodynamics," Phys. Fluids **18**, 111301 (2006).
[19] M. N. Kogan, *Rarefied Gas Dynamics* (Plenum, New York, 1969).
[20] In what follows, the "steady-state" solution for $\omega \gg 1$ refers to the periodic time behavior of the system at late times.
[21] M. Abramowitz, "Evaluation of the integral $\int_0^\infty e^{-u^2-x/u}du$," J. Math. Phys. (Cambridge, Mass.) **32**, 188 (1953).
[22] J. H. Park, P. Bahukudumbi, and A. Beskok, "Rarefaction effects on shear driven oscillatory gas flows: A DSMC study in the entire Knudsen regime," Phys. Fluids **16**, 317 (2004).
[23] N. G. Hadjiconstantinou, "Oscillatory shear-driven gas flows in the transition and free-molecular-flow regimes," Phys. Fluids **17**, 100611 (2005).